

# Design constraints on Cherenkov telescopes with Davies-Cotton reflectors

T. Bretz and M. Ribordy

*High Energy Physics Laboratory, EPFL, CH-1015 Lausanne, Switzerland*

---

## Abstract

This paper discusses the construction of high-performance ground-based gamma-ray Cherenkov telescopes with a Davies-Cotton reflector. For the design of such telescopes, usually physics constrains the field-of-view, while the photo-sensor size is defined by limited options. Including the effect of light-concentrators in front of the photo sensor, it is demonstrated that these constraints are enough to mutually constrain all other design parameters. The dependability of the various design parameters naturally arises once a relationship between the value of the point-spread functions at the edge of the field-of-view and the pixel field-of-view is introduced. To be able to include this constraint into a system of equations, an analytical description for the point-spread function of a tessellated Davies-Cotton reflector is derived from Taylor developments and ray-tracing simulations. Including higher order terms renders the result precise on the percent level.

Design curves are provided within the typical phase space of Cherenkov telescopes. The impact of all design parameters on the overall design is discussed. Allowing an immediate comparison of several options with identical physics performance allows the determination of the most cost efficient solution. Emphasize is given on the possible application of solid light concentrators with their typically about two times better concentration allowing the use of small photo sensors such as Geiger-mode avalanche photo diodes. This is discussed in more details in the context of possible design options for the Cherenkov Telescope Array. In particular, a solution for a 60 mm<sup>2</sup> photo sensor with hollow cone is compared to a 36 mm<sup>2</sup> with solid cone.

*Keywords:* TeV Cherenkov astronomy, Davies-Cotton design parameters, photo-sensors, Winston cone

---

## 1. Introduction

The next generation Cherenkov Telescope Array (CTA) will be constituted of three types of imaging atmospheric Cherenkov telescopes: small-, medium- and large-sized telescopes. The array will be dedicated to the observation of the high energy gamma-ray sky with unprecedented sensitivity [5] over a broad range of energies ( $0.01 \text{ TeV} \lesssim E_\gamma \lesssim 100 \text{ TeV}$ ). This instrument will enable astronomers and astro-particle physicists to refine models of gamma-ray sources and underlying non-thermal mechanism at work, to study the origin and the composition of the cosmic rays up to the knee region, question the nature of the dark matter, etc.

These kind of telescopes detect Cherenkov light emitted along developing showers in the atmosphere nearly uniformly illuminating the ground over an area of about 50'000 m<sup>2</sup>. Shower maxima of a gamma-ray induced electromagnetic shower occur at altitudes comprised between ~7 km and ~12 km, for a primary energy ranging from ~100 GeV to ~100 TeV.

The photon density on the ground depends on the energy of the gamma ray, its incidence direction and the distance from the resulting shower axis. The displacement of the image centroid in the telescope camera is a function of the angular distance of the shower core, defined by shower impact distance and altitude of the shower and is typically about 1.5° for an energy of

1 TeV and an impact parameter of 150 m, and 3° to 3.5° for energies around 100 TeV with an impact parameter of 300 m. As very high energy showers penetrate deeply in the atmosphere and generate a large amount of light, they can be observed at a relatively large distance from the main light pool already with relatively small reflectors translating into the necessity of a deployment of telescopes with large field-of-view for the exploration of very high energy showers. In general, the required telescope field-of view in order to record contained shower images ranges between 3° and 10° depending on the energy range of interest.

A promising design for wide field observations is the Davies-Cotton telescope [17]. Its advantage is a point-spread function enabling a larger field-of-view than a parabolic design. The Schwarzschild-Coudé design (e.g. [16]) is not considered further, as it presents technical and cost challenges compared to a conservative CTA proposal using a prime optics design (see also the comments in section 2.1).

It is demonstrated that once the field-of-view of the camera pixels and of the whole instrument together with the photo-sensor technology is fixed by means of physics arguments, only one parameter is left free. This parameter can be fixed as well, relating the worst optical resolution in the field-of-view, i.e. at the edge of the field-of-view, with the size of a pixel. Having a reasonable cost model at hand, even the most cost-efficient single telescope or telescope design operating in an array can be derived.

---

\*Corresponding author: thomas.bretz@epfl.ch

Knowing the anticipated angular size of a pixel from physics constraints, a requirement on the point-spread function of the telescope can be determined. If the point-spread function is identified by the root-mean-square of the light distribution, requiring a pixel diameter four times the root-mean-square ensures that most of the light from a point source at infinity is concentrated in a single pixel at the edge of the field-of-view.<sup>1</sup> If simulations show that such a containment is not necessary in terms of angular resolution of the shower origin or background suppression, also a smaller value like twice the root-mean-square can be considered, c.f. [1]. If this requirement is not optimized or not met, either the physics outcome is worsened or the camera has more pixels than necessary and will not be cost-efficient.

The CTA array layout will consist of large size telescopes (LST, primary mirror diameter  $\sim 24$  m) in the center, and successively surrounded with an increasing number of medium-sized (MST,  $\sim 12$  m) and small-sized (SST,  $\sim 6$  m) telescopes in order to instrument a ground surface area comprised between  $4 \text{ km}^2$  and  $10 \text{ km}^2$ . Telescope spacings, sizes and field-of-views reflect the energy range to be explored by a certain type of telescope. The LST sub-array will be primarily focusing on the observation of the high energy gamma-ray sky with great precision below about 100 GeV, the inter-telescope spacing will be small, about 60 m and the single telescope field-of-view limited to about  $3^\circ - 4^\circ$ . The SST sub-array will conversely be optimized for multi-TeV observations, up to around 100 TeV allowing for large spacing of up to 300 m – 500 m with relatively modest reflector size. The camera pixel field-of-view of these different telescope types will span between about  $0.08^\circ - 0.1^\circ$  (LST) up to  $0.2^\circ - 0.3^\circ$  (SST), linked to the different shower intensity with its intrinsic fluctuations and the concurrent necessity of keeping the number of camera pixels reasonably low.

Consequently, this study will focus on reflector diameters in the range of a meter to about 30 m and on pixel field-of-views in the range between  $\sim 0.08^\circ$  and  $\sim 0.3^\circ$ . and is extended to off-axis angles of the incoming light up to more than  $5^\circ$ .

In the following, first a description is derived for the relations between the existing design parameters of a Cherenkov telescopes, e.g. focal length and reflector diameter. Then, by including a semi-analytical treatment for the optical quality of a generalized Davies-Cotton reflector, this description becomes applicable for the design of real telescopes. At the end, the influence of the variation of the parameters on the optimized design is discussed.

## 2. Optimization

The light collection is one of the most important parameter of a Cherenkov telescope and can be improved by, e.g., an increase of the photo-detection efficiency of the photo-sensors or a rescaling of the system, i.e., a corresponding rescaling of the reflective area and photo-sensor size. As current technology (photo-multiplier tubes, hybrid photo-detectors or silicon

photo-multipliers) only offer a limited choice of photo-sensor sizes, the Cherenkov telescope design parameter phase space is reduced. Given a particular photo-sensor type, the addition of a light concentrator in front of the photo-sensor is the only way to increase the light collection efficiency.

In the following, it will be shown that the relationship between the characteristic parameters of an optimal telescope design (pixel field-of-view and linear size, reflector diameter and focal distance) is fully constrained, once the technological requirement (photo-sensor size and the light-guide material) and the physics requirements (the pixel angular size and the field-of-view) are frozen. This result is obtained by imposing restrictions on the value of the point-spread function at the edge of the field-of-view in order to keep adequate image quality and thus analysis potential.

### 2.1. Light concentrators

The theorem of Liouville states that the maximum concentration theoretically achievable is defined by maintaining the phase space, i.e. the product of solid angle, defined by the incoming light rays directions, light ray momentum squared and the surface area crossed by the light rays. The theorem of Liouville is applicable to the case of a Winston cone with entrance area  $A$  placed in front of a photo-detector of area  $A'$ , corresponding to the exit area of the cone.  $A$  is defined provided  $A'$ , the solid angle  $\Omega$  defined by the light rays entering the cone and the solid angle  $\Omega'$  defined by the light rays leaving the cone.

Winston has shown in [6] that the maximum concentration factor for a rotationally symmetric light concentrator is

$$C_{max} = \frac{A}{A'} = \left(\frac{n'}{n}\right)^2 \cdot \frac{1}{\sin^2 \phi}, \quad (1)$$

where  $n$  and  $n'$  denote the refractive index of the media in front of and inside the optical system with  $n \approx 1$  in air.  $\phi$  corresponds to the maximum angle at which a light ray enters the system related to the solid angle  $\Omega$ .

If the system is not axisymmetric or the angular acceptance of the photo detector is smaller than  $\Omega' = 2\pi$  (as assumed in Eq. 1),  $C_{max}$  has to be adapted accordingly.

Besides the increase of the light collection area, the use of cones enables a partial screening of the night-sky light pollution corresponding to  $\phi$  being larger than the angle of light rays coming from the edge of the reflector.

Simulations [7] and recent concentration efficiency measurements [8] of solid cones ( $n' \approx 1.4$ ) designed for the FACT camera [9] demonstrated that their shape is nearly ideal, that the concentration factor reaches a value close to  $C_{max}$  and the geometric loss is only of the order of a few percent excluding absorption loss<sup>2</sup>. In the case of hollow cones, Fresnel reflection losses have to be considered at the surface of the photo-sensor. If the camera is sealed with a protective window, which is usually the case, also losses at the window surface need to be taken

<sup>1</sup>In the case of a normal 2D-Gaussian distribution this would correspond to more than 86% of the light distribution.

<sup>2</sup>The cones designed for the FACT camera were designed on the assumption of a later extension of the mirror area, i.e., they were designed for a larger reflector diameter than the currently installed one.

into account. By choosing a material for the cones and the protective window with a similar refractive index than the material of the photo-sensor light entrance, these losses can be omitted. Combined with the almost perfect reflectivity of solid cones due to total reflection (limited only by the surface roughness), solid cone usually outperform hollow cone.

The concentration factor achieved with the Winston cones is fundamentally similar to the size reduction of the focal plane in a Schwarzschild-Coudé design and linked to the conservation of the space-momentum phase space according to the Liouville theorem: the conversion of the spatial into momentum phase space, by means of Winston cones or secondary optics. While cones reduce the acceptance of the incoming light rays from a large area at the entrance to a large angular acceptance and small area at the cone exit, the secondary mirror optics leads to a similar spatial compression and angular widening of the light rays at the photo-sensor and thus a reduced plate-scale. While cones are non-imaging devices, the secondary optics is imaging. Hence, in the Schwarzschild-Coudé design, it is possible to attain excellent optical resolution, in terms of Cherenkov telescope requirements, with a field-of-view as large as  $15^\circ$ . Both designs enable compression of the photo sensitive area by factors larger than ten w.r.t. their primary optics design.

## 2.2. Connection to the optical system

In the case of a Cherenkov telescope, the light entering the cone comes from a reflector visible under a maximum angle  $\phi$ <sup>3</sup>. The opening angle of the light at the entry of the cone is therefore well defined by the properties of the optical system, i.e. by the diameter of the reflector  $D$  and the focal length  $F$ ,  $f = F/D$ .

$$\tan \phi = \frac{1}{2f} \quad (2)$$

Combining this with Eq. 1 yields

$$\frac{A}{A'} = \left(\frac{n'}{n}\right)^2 \cdot (4f^2 + 1). \quad (3)$$

For instance, taking the FACT values,  $n' = 1.4$  and  $f = 1.4$ , we obtain the theoretically maximal achievable concentration factor  $C_{\max} = 17.3$ , i.e. the linear size of the entrance area can ideally be larger than four times the linear photo-sensor size.

## 2.3. The optical system

In addition, the optical system defines the zoom factor or plate-scale, i.e. the field-of-view corresponding to a physical area in the focal plane. The correspondence between the angular size  $\vartheta$  and the linear size  $\delta$  on the focal plane is

$$\tan \frac{\vartheta}{2} = \frac{\delta}{2F} \quad (4)$$

or in the limit of small  $\vartheta$ ,

$$\delta \approx \vartheta F. \quad (5)$$

Cameras in Cherenkov telescopes are pixelized due to the use of photo-detectors. To increase the light collection efficiency further, and to maintain symmetry, these pixels are usually aligned on a hexagonal grid, i.e. in closed package geometry. In recent years, MAGIC has exploited the photon arrival time extracted from the measured pulse and demonstrated significant improvements in the sensitivity [10].

The technique, taking into account the change of the arrival time between neighboring pixels, performs best, if all neighbors are at an identical distance from the central pixel. Consequently, the ideal shape of a pixel is hexagonal.

The distance  $\delta$  on the camera surface is the distance between two parallel sides of a hexagon, its area is

$$A = \frac{\sqrt{3}}{2} \delta^2. \quad (6)$$

Combining with Eq. 3, the plate-scale formula Eq. 4 and Eq. 6,

$$\frac{\sqrt{3}}{2} \left(\frac{n}{n'}\right)^2 \frac{\tan^2(\vartheta/2)}{A'} = \frac{1}{D^2} + \frac{1}{4F^2} \quad (7)$$

is obtained, which translates the close relationship between the pixel field-of-view  $\vartheta$ , the focal length  $F$  and the reflector diameter  $D$ , once the technological parameters fixed: photo detector size  $A'$  and light concentrator material  $n'$ .

Defining a constant related to these properties

$$k(n, n', A') = \frac{\sqrt{3}}{2 \cdot A'} \cdot \left(\frac{n}{n'}\right)^2 \quad (8)$$

and rewriting Eq. 7 ( $\tan \vartheta \approx \vartheta$  for  $\vartheta \ll 1^\circ$ ) as

$$F = \frac{1}{\sqrt{k \vartheta^2 - (2/D)^2}}, \quad (9)$$

it is immediately apparent that the focal length  $F$  of the system is a direct consequence of the pixel field-of-view and the reflector diameter, if the properties of the photon detector and the material of the cones are known. For typical Cherenkov telescopes,  $F/D$  is between unity and two. Below unity the resolution becomes too coarse and above two, not only the number of pixels and hence the price of a camera becomes too high, but also the camera holding structure becomes mechanically complex and hence disproportionately expensive. This constraint on  $F/D$  applied to Eq. 9 yields

$$4.25 < k \vartheta^2 D^2 < 5. \quad (10)$$

Precisely the choice of  $F$  and  $D$  defines the optical quality of a mirror system. At the same time, the size of a single pixel defines a natural constraint on the optical quality of a system, i.e.,  $F/D$  should be chosen such that the point-spread function at the edge of the camera is within a limit well defined by the pixel's field-of-view.

## 2.4. Optical quality

The light collection area is important for a Cherenkov telescope and typical reflector sizes range from a few to ten or

<sup>3</sup> $\phi$  defined from the focal plane center

twenty meters. However, with the current technology, it is not possible to produce large mirrors with the requested quality at a reasonable cost. Furthermore, optical systems compiled from a single mirror suffer large aberration effects at large off-axis angles, while a wide field-of-view is necessary for the observation of multi-TeV showers up to large impact parameters, as well as for extended sources. Therefore, segmented mirrors are in use. The layout providing the best optical quality for segments of identical focal length is the so-called Davies-Cotton layout [15], where the single spherical mirrors are located on a sphere with radius  $F$  and focused to a point at  $2F$ .

The relevant quantity which influences the on-axis and off-axis optical quality is the focal ratio  $F/D$ . The optical quality improves with larger values. This scale invariance statement is true only as long as the optical quality of a single mirror can be neglected against the optical quality of the whole system, which is generally the case at the edge of the camera.

To be able to constrain the optical point-spread function, a relation between the tessellation, the focal ratio and the resulting point-spread function is needed for a given maximum inclination angle of the light, i.e. at the edge of the field-of-view of the camera.

In Appendix A.1, a formalism describing the point-spread function of an ideal Davies-Cotton reflector, i.e. a reflector with infinite tessellation is presented. The point-spread function is described by the root-mean-square of the light distribution. With the help of ray-tracing simulation, a reasonably good description of a real tessellated Davies-Cotton reflector is derived from this analytical approach in Appendix A.2. Including the correction factor which describes the deviation of the analytical approach from the simulations, a good description of the point-spread function is obtained. It is shown that the point-spread function  $P$  of an ideal Davies-Cotton can be expanded into a polynomial in  $\alpha^i \cdot f^{-j}$ . Given the incident angle  $\alpha \ll 1$  of the incoming ray and  $f$  in the range between one and two, the polynomial is hypothesized into the more simpler form

$$P(f, \alpha, N) = c_0(\alpha, N) \cdot f^{-c_1(\alpha, N)} \quad (11)$$

with coefficients  $c_0$  and  $c_1$  and  $N$  the tessellation number as described in Appendix A.2. This parametrization is found to match the ray-tracing simulation without loss of precision. The coefficient  $c_0$  can directly be deduced as the result of Eqs. A.11 at  $f = 1$  and  $c_1$  is derived by a fit. An example for the coefficients  $c_0$  and  $c_1$  for selected  $\alpha$  is shown in Fig. 1.

### 2.5. Result

As discussed in the introduction, it is required that the point-spread function is small compared to the pixel field-of-view at the edge of the field-of-view, so that the light of a point source is well contained in one pixel. Defining the ratio  $r$  between both, this requirement can be expressed as

$$\vartheta = r \cdot P. \quad (12)$$

Combined with Eq. 11, the focal ratio  $f$  can now be expressed as

$$f = \left( \frac{\vartheta}{r \cdot c_0} \right)^{-\frac{1}{c_1}}. \quad (13)$$

Including this in Eq. 9 yields

$$D^2 = \frac{4g}{k} \vartheta^{-2} \quad (14)$$

with a correction factor  $g$  defined as

$$g = 1 + \frac{1}{4} \left( \frac{\vartheta}{r \cdot c_0} \right)^{\frac{2}{c_1}}. \quad (15)$$

The absolute focal length  $F$  can now be calculated using Eq. 9.

To deduce the effective reflective area from Eq. 14, the shadow of the camera on the reflector has to be taken into account. To calculate the fraction of the reflector shadowed, the ratio of their areas is calculated. Conversion of  $\alpha$  from an angle to a length yields approximately  $R = F \cdot \alpha$  for small values of  $\alpha$  ( $\ll 10^\circ$ ).

Expressing the focal length by Eq. 13 the fraction of the camera shadow on the reflector is derived.

$$\frac{A_{cam}}{A_{ref}} = \frac{\pi F^2 \alpha^2}{\pi \left(\frac{D}{2}\right)^2} = (2\alpha f)^2 = \frac{\alpha^2}{g-1} \quad (16)$$

If a real camera housing is significantly larger than the photo sensitive area itself, a correction factor should be included.

Now the effective light collection area of the optical system can be deduced as

$$A_{eff} = \frac{\pi g}{k} \left( 1 - \frac{\alpha^2}{g-1} \right) \vartheta^{-2}. \quad (17)$$

If real setups should be compared, like e.g. Davies-Cotton and Schwarzschild-Coudé, also other sources of light-losses must be included, such as geometrical efficiency of the cones (light-loss at the edge of the mirror), total mirror reflectivity, cone transmission or reflection losses, or photo detection efficiency.

### 2.6. Discussion

The relation given in Eq. 14 includes several parameters which are subject to change. For simplicity, a standard setup has been defined to which altered setups are compared.

Silicon photo-detectors are a recent and very promising technology. Therefore, a silicon photo-detector with a sensitive area of 36 mm<sup>2</sup> is chosen as a benchmark device. Such devices are already commercially available with acceptable properties. Although their sensitive area is still rather small compared to photo-multipliers, by increasing their light-collection with solid light concentrators, their light-collection area becomes reasonably large. Such light-concentrators still maintain a reasonable weight and length in term of absorption. Typical Plexiglas materials have a refractive indices of the order of  $n'=1.4$  and are used hereafter as a reference.

As the light-collection area of a telescopes scales directly with the photo-sensitive area, the most obvious use of small photo sensors is a small telescope sensitive mostly to high energetic showers. At high energies, the collection area of a telescope array is of prime importance due to rapidly decreasing

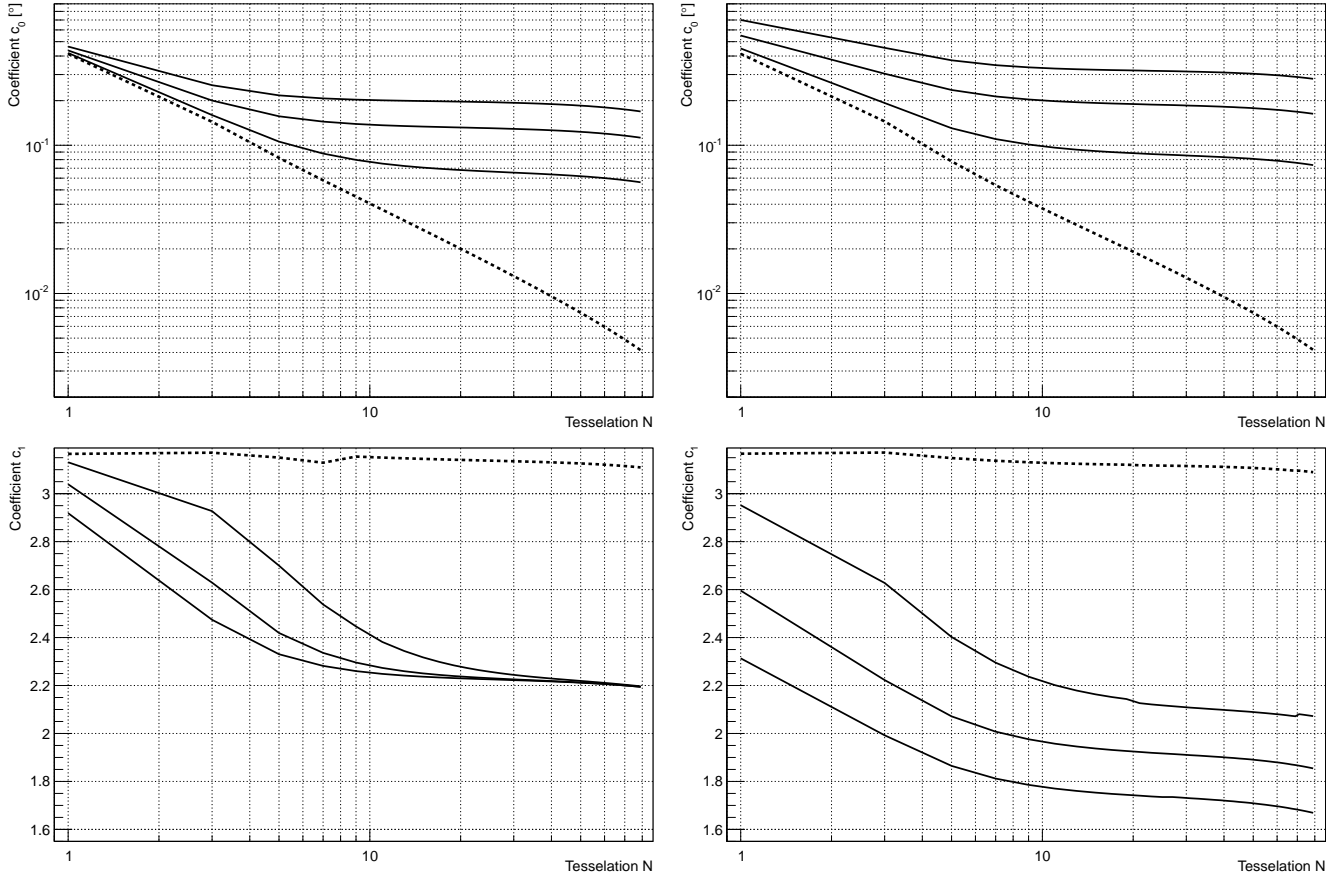


Figure 1: Coefficients derived from the work in the Appendix to convert the focal ratio  $f$  into point-spread function as defined in Eq. 11. Sagittal component (left) and the tangential component (right). The dashed line denotes on-axis rays  $\alpha=0^\circ$ , the solid lines (from the dashed line outwards) rays at  $2^\circ$ ,  $4^\circ$  and  $6^\circ$  off-axis.

fluxes. Due to the bright light-pool of high energy showers, telescopes with relatively small reflectors can be operated with large spacing of, e.g., 400 m or more, c.f. [2]. Since such spacings demand a large camera field-of-view, a field-of-view of  $9^\circ$  diameter is chosen as a reference.

A typical reflector for a Cherenkov telescope with Davies-Cotton layout enables the manufacturing of a primary reflector tessellated into spherical mirror of identical focal lengths. From the scaling with the tessellation number as derived in A.11, it can be concluded that a layout with only three mirrors on the diagonal ( $N=3$ ) has still a significantly worse optical quality than a reflector with five mirrors on the diagonal. Although the point-spread function at the center of the camera is clearly dominated by the mirror size, the relative influence almost vanishes at higher off-axis angles. Since the solution with  $N=3$  still shows a degradation of more than 10% compared to the solution with  $N=5$  even at the highest simulated off-axis angles, it is discarded. On the other hand, a further increase of the tessellation number (individual mirror size over primary reflector diameter) does not significantly improve the optical quality. Consequently, choosing  $N=5$  is a good compromise and already close to the optimum achievable. Comparable results were obtained in [4] although using a third order approximation overestimating the optical quality.

It must be noted that the simulation does not take the point-spread function of the individual mirrors nor any possible misalignment into account which must be added quadratically to the result. However, for the solutions discussed here this can be neglected, c.f. [3]. In general, alignment errors can be kept minimal and individual mirrors can be machined with a point-spread function small compared to the point-spread function at the edge of the camera.

On average, all Davies-Cotton designs with a reasonable  $F/D$  have a root-mean-square of the light distribution in the tangential direction about two times larger than in the sagittal direction.

Ideally, the sagittal root-mean-square at the edge of the camera should fit a fourth of the pixel's field-of-view. This ensures that in the sagittal direction 95% of the light is contained within one pixel diameter and roughly 68% in the tangential direction. However, since the point-spread function is not Gaussian and has long tails in tangential direction exact numbers for the light content might slightly differ.

For convenience, all following plots show dots for  $F/D = \{1, 1.25, 1.5, 1.75, 2\}$ .

Fig. 2 shows the reflective area versus the pixel's field-of-view for comparison in the standard case with and without shadowing for different camera field-of-views. Since the effect

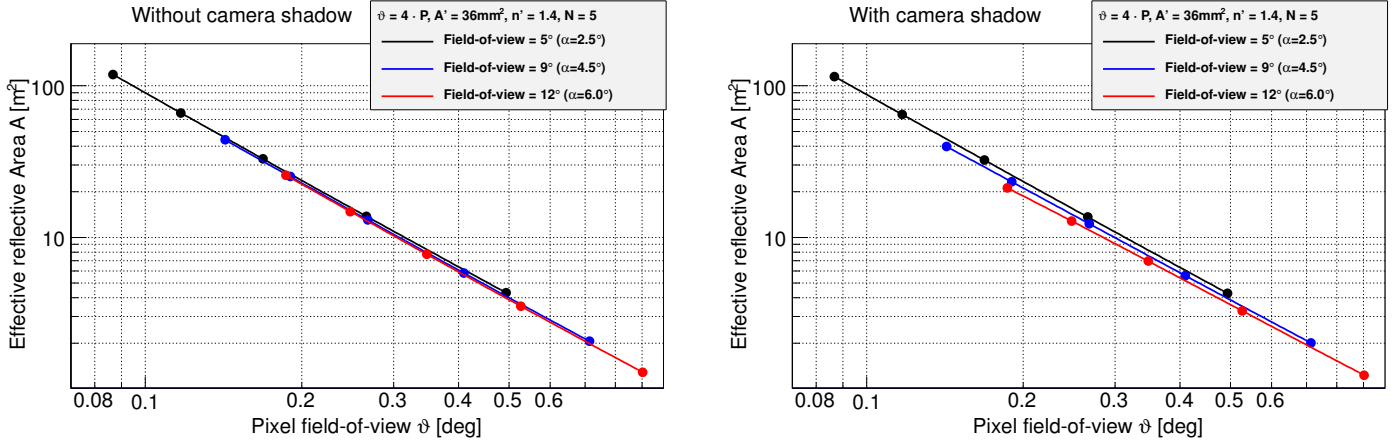


Figure 2: Reflective area (left) and the effective reflective area (right), i.e. including the camera shadow, for the standard setup as discussed in section 2.6. The result is shown in the range between  $F/D = [1, 2]$ . The dots denote intermediate results at  $F/D = \{1.25, 1.5, 1.75\}$ . For convenience the result is also shown for a camera field-of-view of  $5^\circ$  and  $12^\circ$ . The legend gives the corresponding pixel field-of-view  $\vartheta$  with its relation to the optical point-spread function  $P$  at the edge of the camera, the photo sensitive area  $A'$  of the photo sensor, the refractive index  $n$  of the light collector and the tessellation of the reflector expressed as the number  $N$  of individual mirrors on its diagonal.

is comparably small and the mirror diameter is more expressive, in the following all plots show the mirror diameter rather than the reflective surface in the non-obstructed case.

The effects of changing different input parameters w.r.t. to the previously described benchmark configuration are shown in Fig. 3 and discussed below.

*Changing the camera field-of-view (Fig. 3, top plot).* Changing the camera's field-of-view basically shifts the valid range along the line, i.e. the range corresponding to  $F/D = [1.0, 2.0]$ . That means that it is possible to build telescopes identical in optical quality, pixel's field-of-view and mirror diameter, but different field-of-view resulting simply in a different focal length of the system. In short: Changing the field-of-view only changes the focal length.

*Changing the optical quality (Fig. 3, middle plots).* A change in the requirement on the optical quality  $r$  directly influences  $F/D$ , and therefore also shifts the range of reasonable  $F/D$  almost linearly in  $\vartheta$  (left plot). Changing the tessellation (right plot) is like changing the requirement on the optical quality. While the difference in optical quality between a Davies-Cotton layout with three mirrors on the diagonal and five mirrors is still significant, all other layouts give identical results within a few percent. In short: Any tessellation number  $\geq 5$  gives similar results. Changing the requirement on the optical quality only changes the focal length.

*Changing the photo sensitive area (Fig. 3, bottom left plot).* Since the constant  $k$  is directly proportional to the size  $A'$  of the photon detector, the mirror area is directly proportional to the size of the photo sensor. If the size of the photon sensor is limited, a simple way to increase the field-of-view of a single pixel is to sum the signal of several photon counters to a single signal. To maintain a hexagonal, i.e. most symmetric layout, summing the signal of three, four or seven photon sensors seems appropriate. In short: Assuming an optimized light-concentrator, the photo sensor's physical size defines the scale of the system.

*Changing the light concentrator (Fig. 3, bottom right plot).* Another way to increase the reflective area is an increase of the refractive index of the light concentrator entering quadratically. Using solid cones made from a Plexiglas material with a typical refractive index in the order of 1.4 allows to increase the achievable reflective area by a factor of two compared to hollow cones. Since the length of a typical light concentrator for an exit of 1 mm diameter is in the order of 3 mm – 4 mm, weight and light-attenuation, which is dependent on the length of the material crossed, will define a natural limit on the sensor size for which a solid cone is still efficient. For comparison reasons not only solid ( $n'=1.4$ ) cones but also intentionally less efficient hollow cones ( $n=1.0$ ) are shown. Non-optimum hollow cones are typically used in current Cherenkov telescopes, in which the sensitive area of standard photo-detectors (PMTs) is not a limiting factor. In short: Increasing the refractive index, quadratically increases the reflective area of the system.

Another interesting aspect for the final performance of a telescope is the collection of background photons from the diffuse night-sky background. Here, Eq. 17 leads to an interesting conclusion. Since the rate of the night-sky background photons per channel scales with the effective reflective area and the solid angle corresponding to the field-of-view of the pixels, the night-sky background rate  $R$  is proportional to

$$R \propto A_{eff} \cdot 4\pi \sin^2 \frac{\vartheta}{2} \approx A_{eff} \cdot \pi \vartheta^2, \quad (18)$$

yielding

$$R \propto \frac{\pi^2 g}{k} \left(1 - \frac{\alpha^2}{g-1}\right). \quad (19)$$

For the range of  $F/D = [1, 2]$ , Eq.13 and Eq. 15 yield a correction factor  $g$  between 1.0625 and 1.25. With them, Eq. 19 can be transformed into  $R \propto c/k$ , with Eq. 8 into  $R \propto c' A' n^2$ . It is immediately apparent that the night-sky background rate scales with the physical entry area of the pixel. Assuming only reasonable camera field-of-views between  $3^\circ$  and  $13^\circ$  diameter,

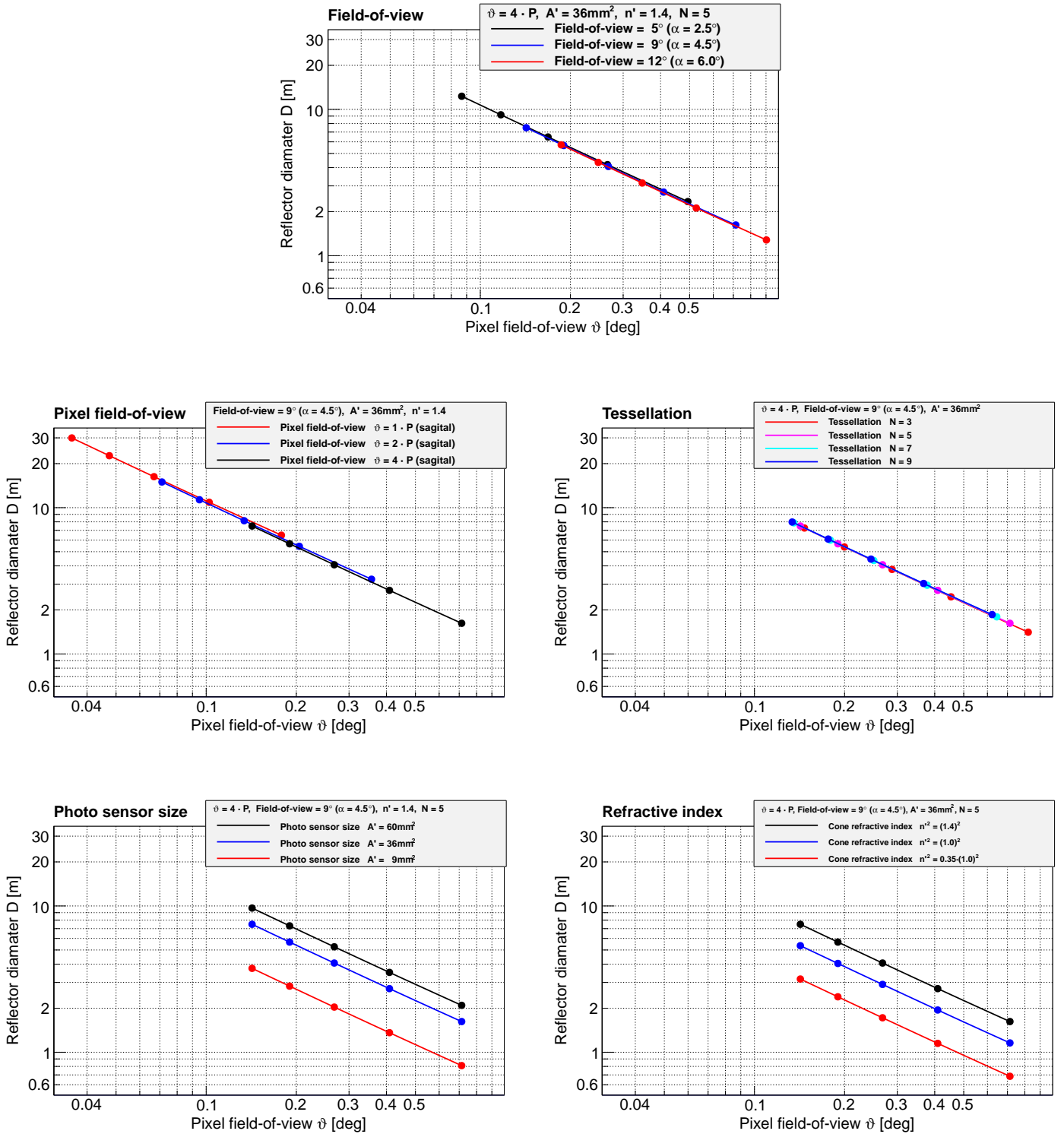


Figure 3: Reflector diameter versus pixel's field-of-view for different setups. The results are shown in the range between  $F/D = [1, 2]$ . The dots denote intermediate results at  $F/D = \{1.25, 1.5, 1.75\}$ . For convenience the result is also shown for a camera field-of-view of  $5^\circ$  and  $12^\circ$ .

the coefficient  $c' = 2/\sqrt{3}c$  is between 9.6 and 14.2. This can be interpreted such that the night-sky background rate per pixel can be considered constant within  $\pm 10\%$  in the first order along the lines of an optimized telescope. The dependence of  $c'$  on  $F/D$  and the camera field-of-view is shown in Fig. 4.

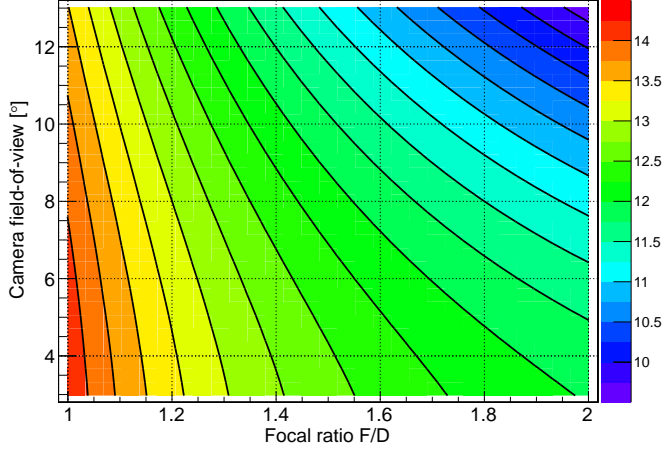


Figure 4: The color coded coefficient  $c'$  describing the scale of the night-sky-background rate versus focal ratio  $F/D$  and camera field-of-view (diameter) for fixed cone material and photo detector size.

Quantitatively the night-sky background rate  $r_{\text{NSB}}$  is given by

$$r_{\text{NSB}}(r_{\text{pixel}}, A_{\text{mirror}}, \chi(\nu), f(\nu)) = \pi r^2 A_{\text{mirror}} \int d\nu \frac{f(\nu)}{E_\nu} \chi(\nu)$$

where  $\chi(\nu)$  and  $f(\nu)$  are the photo-sensor's photo-detection efficiency and the night-sky background intensity, respectively. For silicon photo detectors (MPPC [12]), as used in the FACT camera, and the night-sky background at La Palma [13],  $r_{\text{NSB}}$  is about 150 MHz (much larger than the device dark count rate) given a reflective area of  $10 \text{ m}^2$  and a pixel field-of-view of  $0.2^\circ$ . If a cutoff in the photo-detection efficiency is introduced at 650 nm (PMT-like behavior), this can be further reduced. In general, the night-sky background rate is not a main problem in Cherenkov astronomy, as the combined trigger requirements of signal among nearest pixel neighbors and within a short time lead to its very efficient suppression.

*General considerations.* Existing telescopes are usually under-designed, i.e. the photo-detectors are larger than necessary or the light-concentrators do not reach the maximum possible concentration.

On the contrary, currently so-called Silicon Photo-multipliers have proven their potential in Cherenkov telescopes [11]. These silicon based photo-detectors usually have a very limited area, but used in an optimized setup, their effective physical light collection area, i.e. entry of the light concentrator, can be much larger. If prices of photo-sensors are compared, this has to be taken into account. Not the price per  $\text{mm}^2$  physical sensitive area, but the price per cone entrance area or field-of-view, has to be considered. If cheap enough, the signal of several photo-detectors, equipped with individual light concentrators, could even be summed.

For a comparison, in terms of effective reflective area, the transmission losses of solid cones and their gain from avoiding Fresnel reflection has to be taken into account, as well as the reflection losses of hollow cones.

*A note on timing.* For an ideal Davies-Cotton reflector, the arrival time distribution of an instantaneous parallel beam flash is practically flat. More precisely, it is linearly decreasing, but looks flat on the small interval. The number of photons in the arrival time interval  $[T, T + \delta T]$  is  $N(T, \delta T) \propto T$ . Its width  $\delta T$  is given by  $D/c \cdot f_{\text{DC}}(0.5, 0)$ , where  $c$  is the speed of light. The interval is of the order 1.1 ns for a 4 m class reflector ( $F/D \sim 1.5$ , up to slightly less than 4.5 ns for a 12 m reflector considering  $F/D \sim 1.2$ ). This short time spread is not a problem for the observation of showers with a small size telescope as it is still small compared to the Cherenkov light flash duration. For medium and large size telescopes, a slightly different mirror arrangement should be chosen if time spread matters. By a mirror arrangement, intermediate between a spherical (Davies-Cotton) and a parabolic design, the time spread can considerably be improved, maintaining the point-spread function almost completely. While the point-spread function is dominated by the majority of the mirrors, i.e. outermost mirrors, the time spread is dominated by the ones with the largest  $\Delta T$  mirrors, i.e. innermost mirrors. Consequently, moving the innermost mirrors closer to a parabola immediately improves the time-spread while the effect on the point-spread function is rather limited. Ideally, mirrors on a parabola with adapted focal lengths are used, but might be a cost issue. With adapted focal lengths, all mirrors are placed at correct focal distance, so that, a similar point-spread function than for the Davies-Cotton arrangement can be expected.

*Remarks about CTA.* Recent results of FACT [11] show that a reflector in the order of 3.5 m diameter can give already reasonable physics results with current analysis and detector technology. Therefore, a 4 m diameter reflector for SST is assumed. For physics reason, the field-of-view is supposed to be between  $9^\circ$  and  $12^\circ$  (leading to a reasonable  $F/D$  between 1.5 and 1.8 assuming an optical quality of 4 and a tessellation number of 5). Requiring a pixel field-of-view in the order of  $0.26^\circ$ , possible solutions could be solid cones with a  $36 \text{ mm}^2$  G-APD or hollow cones with a  $60 \text{ mm}^2$  G-APD, see also Fig. 5.

The manufacturing of  $60 \text{ mm}^2$  G-APDs is under discussion with Hamamatsu. A rough estimate shows that a solid cone for such a device would be about three times longer than for a  $9 \text{ mm}^2$  as used in FACT. Considering the transmission loss of 10% in the FACT cones [8], which is a very conservative estimate, such cones would have a loss in the order of 35%. Since solid cones avoid the loss from Fresnel reflection at the sealing surface and the G-APD surface, the real light loss would only be around 27% assuming that the hollow cone has a reflectivity of 100% which in reality is not true.

Keeping the pixel field-of-view constant, the gain in reflective area corresponds to the refractive index of the cone material squared. In the case of a refractive index of typical Poly(methyl

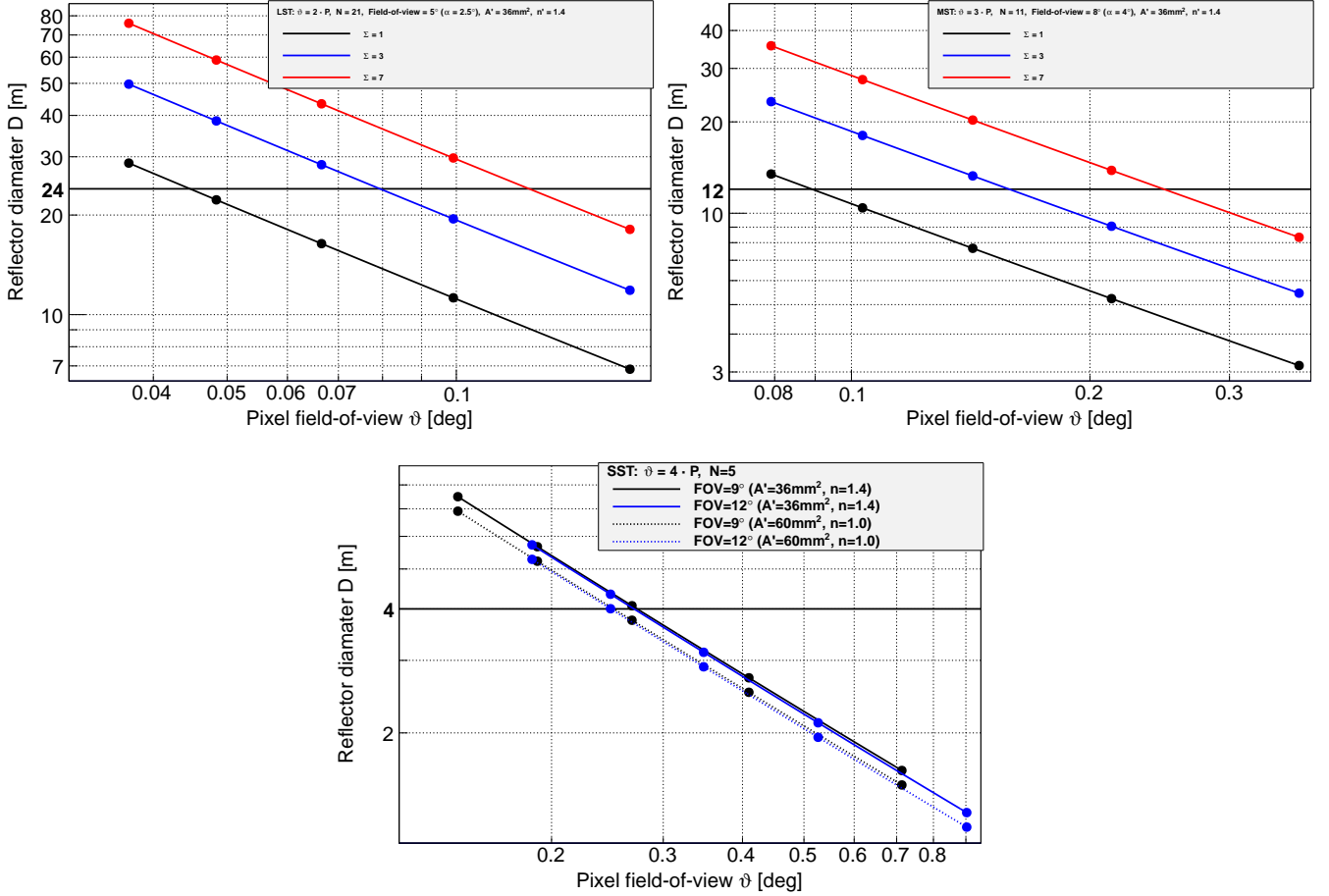


Figure 5: Reflector diameter versus pixel’s field-of-view for selected setups. The shown setups were chosen such that a small-size, medium-size and large-size telescope is considered. The horizontal black lines are to guide the eye to possible setups like  $D=3.5$  m or  $D=5$  m,  $D=12$  m and  $D=24$  m. The displayed range is between  $F/D=[1,2]$ . The dots denote intermediate results at  $F/D=\{1.25, 1.5, 1.75\}$ . The Greek letter  $\Sigma$  denotes the number of photo sensors compiled into a single pixel.

methacrylate) PMMA of 1.4 this is a gain of  $\approx 100\%$  reflective area, which outperforms the transmission loss significantly.

Assuming that the manufacturing of a  $36\text{ mm}^2$  G-APD would be as easy as of a  $60\text{ mm}^2$  G-APD, one can compare a solution with a  $36\text{ mm}^2$  G-APD and a solid cone and a  $60\text{ mm}^2$  hollow cone (assuming perfect reflectivity). In this case, the transmission loss of the solid cone is around 13% compared to 8% Fresnel loss for the hollow cone. On the other hand, the solution with the hollow cone yields a 15% smaller reflective area (same pixel field-of-view) or 27% more pixels (same reflective area).

Assuming further that the price of the camera scales with the price of each channels, a reduction of the number of channels by almost 30% reduces the costs for the camera significantly. Since the costs are also dominated by the price for the photo-detectors, and the price of G-APDs, in the first order, scales with the sensitive area, it can be estimated that the price for the  $36\text{ mm}^2$  G-APDs would be almost a factor of two lower than for the larger ones.

In Figure 5 possibly solutions for MST and LST designs are shown using G-APDs and solid cones. On both cases it is convenient to sum at least three, or even seven, pixels into one read-out channel to keep the ratio  $F/D$  low for construction reasons.

### 3. Conclusion

The Davies-Cotton design with its simplicity as compared to non validated dual optic systems is assuredly a good option for a wide field-of-view, up to  $10^\circ - 12^\circ$ , high energy Cherenkov telescope.

With this study, it is possible to scan a wide phase space of the design of Cherenkov telescopes or telescope arrays. This was achieved by a description of the optical performance of Davies-Cotton reflectors and introduction of the effect of light-concentrators. In particular, this study provides an analytical description of the optical performance of a tessellated Davies-Cotton reflector precise enough to enable performance studies without the need for dedicated simulations.

By including the effect of the light-collector into the system of equations, the available phase space of design parameters is reduced to a single parameter, once the photon detector has been chosen and either the pixel field-of-view or the camera field-of-view has been fixed by physics constraints. While the choice of photo sensor is usually defined by the availability on the market, constraints on the camera field-of-view are a result of the physics targets.

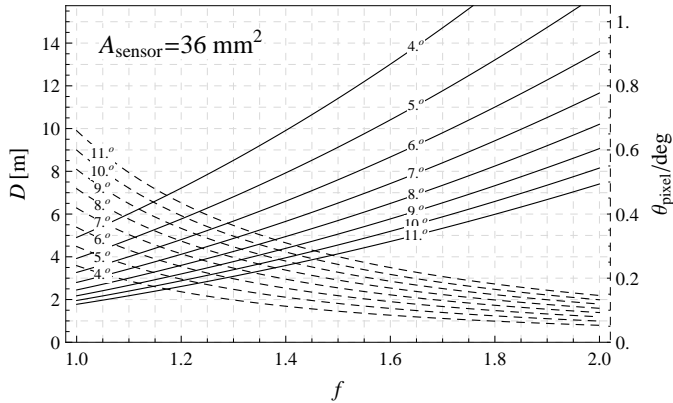


Figure 6: Example design overview for a small size telescope calculated for an ideal Davies-Cotton reflector, i.e.  $N \sim 9$ , a pixel size four times the point-spread function and solid cones with  $n = 1.4$ . For a given  $F/D$  and camera field-of-view, the corresponding reflector diameter and the pixel field-of-view can be read.

If these two parameters are fixed, the whole available phase space of possible solution can now be scanned by changing a single input parameter. It can, for example, be convenient to scan a reasonable range of the focal ratio  $F/D$  and derive all other parameters accordingly. From the result, the most cost efficient solution, or the one performing best in sense of physics targets can be chosen.

For the Cherenkov telescope array, several design options were presented. It could be shown that for the small size telescope, considering a camera field-of-view of  $9^\circ$  to  $12^\circ$ , a four meter reflector is enough if  $36 \text{ mm}^2$  sensors are topped with solid cones to achieve a pixel field-of-view in the order of  $0.25^\circ$  to  $0.3^\circ$  at reasonable  $F/D$ . An alternative solution are hollow cones with correspondingly larger sensor area, which is disfavored because of the costs dominated by the sensor. An example plot which easily allows to determine reasonable options from the available phase space is shown in Fig. 6. The reflector diameter can easily be re-scaled linearly with the photo sensor size and the refractive index of the cone material.

For the medium size and large size telescopes, the most reasonable solution using small sensors would be the summation of three and seven, respectively. Equipped with different sum-stages, these modules could be applied in any telescopes. Larger silicon based sensors, expected soon on the market, would allow a single-channel/single-sensor solution. Using several small sensors in one channel has the advantage that the application of solid cones is possible in terms of weight and transmission and costs for photo sensors can be kept low due to their at least two times higher compression ratio.

## Appendix A. Parametrizing a Davies-Cotton reflector

### Appendix A.1. Ideal Davies-Cotton reflector

The Davies-Cotton design [15] is known to be promising for wide field prime-focus telescopes and was studied earlier analytically [16] and through simulations [17]. However, the parametrizations are moderately accurate and non existing for tessellated reflectors.

Here, parametrizations are provided, accurate at the percent level up to  $12^\circ$  field-of-view, for the ideal (non-constructable) Davies-Cotton telescope and accurate to a few percent for a realistic Davies-Cotton telescope with arbitrary tessellation of the reflector.

*Prime-focus telescope design.* The major issue of the design of a telescope is the reflector and its optical performance. Since design parameters like the field-of-view of a single pixel or the field-of-view of the whole camera are closely related to the reflectors optical performance, it is important to understand the relation between the reflector design and its performance. Unfortunately, neither spherical nor parabolic mirrors can provide both, good optical point spread function for on-axis and inclined rays, at the same time, because the distance between any point on the mirror surface to the focal point does not match the local focal length defined by the local radius of curvature. Furthermore, in the case of a spherical mirror, also the shape of the mirror surface is not ideal compared to a parabolic mirror. The parabolic shape ensures that parallel rays from infinity are well focused into a single point (due to the definition of a parabolic surface) while in the spherical case this is not the case. That means that in both cases rays hitting the mirror far off its center have their focal point not at the focal plane. In the case of a spherical mirror they also miss the focal point (*aberration*).

Consequently, the ideal mirror would be a combination of two properties: A mirror surface which is shaped such that it has the right focal distance at any point, but at the same time any point is correctly oriented, so that focal distance and direction are correct. Since local normal vector and local curvature cannot be disentangled such a mirror can only be a theoretical construction. Tessellating the reflector into individual mirrors, this behavior can be approximated, as shown by Davies and Cotton, if the reflector is built from several spherical mirrors which are placed on a sphere around the focal point. In this case, the reflector can have the correct focal distance locally and, at the same time, the mirror elements can be oriented such that they correctly focus to the focal point. Apart from an improved optical performance for inclined rays, the production of several small and identical mirrors is also much more cost efficient than the production of a single large mirror.

Since any optical system can always be linearly scaled, in the following a scale factor is chosen such that the reflector diameter corresponds to unity, which is identical to defining  $f = F/D$  with  $F$  being the focal length and  $D$  the diameter of the mirror.

*Spherical reflector.* The spherical mirror has its focal point at half its radius of curvature  $f$ . Its surface is given by  $z =$

$f_{\text{sph}}(x, y)$  and its normal vector by  $\vec{n}_{\text{sph}}(x, y)$ :

$$f_{\text{sph}}(x, y) = 2f - \sqrt{(2f)^2 - (x^2 + y^2)} \quad (\text{A.1})$$

$$\vec{n}_{\text{sph}}(x, y) = (x/(2f - f_{\text{sph}}), y/(2f - f_{\text{sph}}), -1) \quad (\text{A.2})$$

*Ideal Davies-Cotton reflector.* The ideal Davies-Cotton reflector has a non constructable surface. Its shape  $z = f_{\text{DC}}(x, y)$  is spherical with radius of curvature  $f$ , but its normal vectors are defined to intercept at location  $\vec{F} = (0, 0, 2f)$ . Formally, the surface equation  $f_{\text{DC}}(x, y)$  and the surface normal vectors  $\vec{n}_{\text{DC}}(x, y)$  are

$$f_{\text{DC}}(x, y) = f - \sqrt{f^2 - (x^2 + y^2)} \quad (\text{A.3})$$

$$\begin{aligned} \vec{n}_{\text{DC}}(x, y) &= \nabla(f_{\text{DC}}(x, y) - z) \\ &= \left( \frac{x}{2f - f_{\text{DC}}(x, y)}, \frac{y}{2f - f_{\text{DC}}(x, y)}, -1 \right) \end{aligned} \quad (\text{A.4})$$

Practically, this equations describes infinitely small mirror elements placed on a sphere, oriented accordingly.

*Taylor development.* To have the root-mean-square of the projection of reflected rays on the focal plane along  $x$  and  $y$  coinciding with tangential and sagittal resolutions, a rotation around  $z$  is performed without loss of generality.

An incoming ray with vector  $\vec{v} = (0, \sin \phi, \cos \phi)$  will therefore be reflected on the surface in the direction  $\vec{v}_r = \vec{v} - 2(\vec{v} \cdot \vec{n})\vec{n}/n^2$  and intercept the (non curved) focal plane at  $r = \sqrt{x^2 + y^2}$ , generally yielding

$$(X, Y, Z) = \left( x + \frac{v_{rx}}{v_{rz}}(f - f(x, y)), y + \frac{v_{ry}}{v_{rz}}(f - f(x, y)), f \right). \quad (\text{A.5})$$

For the ideal Davies-Cotton this takes the explicit form

$$(X, Y, Z)_{\text{DC}} = \left( x + \frac{v_{rx}}{v_{rz}} \sqrt{1 - \frac{r^2}{f^2}}, y + \frac{v_{ry}}{v_{rz}} \sqrt{1 - \frac{r^2}{f^2}}, f \right). \quad (\text{A.6})$$

It is straightforward to numerically calculate the image centroid  $(\bar{\xi}, \bar{\eta})$  and the resolution  $(\Delta\xi, \Delta\eta)$  of such a telescope and to estimate the contribution of various terms to the resolution with a Taylor development of  $X$  and  $Y$  in terms of  $x$ ,  $y$  and  $\phi$ . The development of terms of the form  $x^i y^j \phi^k$ , with  $i + j \leq 5$  and  $k \leq 3$  was found to be sufficient for a percent precision in the resolution parameters.

The tangential and sagittal barycenter in the focal plane (the image centroid) for a uniform beam on the primary surface are given by

$$\begin{aligned} \bar{\xi} &= \frac{\int_0^{1/2} r \, dr \int d\theta Y(x = r \cos \theta, y = r \sin \theta)}{\int_0^{1/2} r \, dr \int d\theta}, \\ \bar{\eta} &= \frac{\int_0^{1/2} r \, dr \int d\theta X(x = r \cos \theta, y = r \sin \theta)}{\int_0^{1/2} r \, dr \int d\theta}, \end{aligned} \quad (\text{A.7})$$

	sph.	DC	sph. 3 <sup>rd</sup> order [17]	DC approx. from [16]
$c_{0,6}^{\xi,\eta}$	$\frac{1}{2^{11}}$	0	$\frac{1}{2^{11}}$	0
$c_{0,8}^{\xi,\eta}$	$\frac{3^2}{2^{14}5}$	0	0	0
$c_{0,10}^{\xi,\eta}$	$\frac{7 \cdot 13}{2^{23}}$	0	0	0
$c_{2,4}^{\xi}$	$\frac{7}{2^5 3}$	$\frac{1}{2^6}$	$\frac{7}{2^5 3}$	$\frac{1}{2^6}$
$c_{2,6}^{\xi}$	$\frac{131}{2^{11} 3}$	$\frac{5}{2^{10}}$	0	$-\frac{1}{2^8}$
$c_{2,8}^{\xi}$	$\frac{257 \cdot 307}{2^{19} 3^2 5}$	$\frac{191}{2^{16} 5}$	0	0
$c_{4,2}^{\xi}$	1	1	1	1
$c_{4,4}^{\xi}$	$\frac{7}{2^4}$	$\frac{5 \cdot 7}{2^5 3}$	0	$\frac{5 \cdot 7}{2^5 3}$
$c_{4,6}^{\xi}$	$\frac{1163}{2^{10} 3^2}$	$\frac{5 \cdot 67}{2^{10} 3}$	0	0
$c_{4,8}^{\xi}$	$\frac{19 \cdot 67 \cdot 1039}{2^{19} 3^2 5}$	$\frac{8527}{2^{15} 3 \cdot 5}$	0	0
$c_{2,4}^{\eta}$	$\frac{1}{2^5 3}$	$\frac{1}{2^5 3}$	$\frac{1}{2^5 3}$	$\frac{1}{2^5 3}$
$c_{2,6}^{\eta}$	$\frac{1}{2^8}$	$\frac{3}{2^{10}}$	0	0
$c_{2,8}^{\eta}$	$\frac{19}{2^{12} 5}$	$\frac{29}{2^{13} 5}$	0	0
$c_{2,10}^{\eta}$	$\frac{5 \cdot 1459}{2^{24} 3}$	$\frac{5 \cdot 53}{2^{21}}$	0	$\frac{3}{2^{10}}$
$c_{4,4}^{\eta}$	$\frac{1}{2^4 3^2}$	0	0	$\frac{1}{2^4 3^2}$
$c_{4,6}^{\eta}$	$\frac{5}{2^{10}}$	0	0	0

Table A.1: Table of coefficients  $c_{i,j}$  for Eq. A.9 and A.10

and the corresponding resolution in term of root-mean-square:

$$\begin{aligned} \Delta\xi^2 &= \frac{\int_0^{1/2} r \, dr \int d\theta (Y(x = r \cos \theta, y = r \sin \theta) - \bar{\xi})^2}{\int_0^{1/2} r \, dr \int d\theta}, \\ \Delta\eta^2 &= \frac{\int_0^{1/2} r \, dr \int d\theta (X(x = r \cos \theta, y = r \sin \theta) - \bar{\eta})^2}{\int_0^{1/2} r \, dr \int d\theta}. \end{aligned} \quad (\text{A.8})$$

The upper integration bound in  $r$  originates from the fact that the optical system was scaled to meet a reflector mirror of  $d = 1$ , hence  $r = 1/2$ .

Taylor development of the above formulas brings the desired result

$$\Delta\xi^2 = \frac{1}{2^4} \sum_{i,j} \frac{c_{i,j}^{\xi}}{f^j} \phi^i, \quad (\text{A.9})$$

$$\Delta\eta^2 = \frac{1}{2^4} \sum_{i,j} \frac{c_{i,j}^{\eta}}{f^j} \phi^i. \quad (\text{A.10})$$

Coefficients given in Table A.1. For the ideal Davies-Cotton, only leading terms  $\frac{c_{i,j}^{\xi}}{f^j} \phi^i$  and  $\frac{c_{i,j}^{\eta}}{f^j} \phi^i$  are retained, at  $f = 1$  and a maximum off-axis angle of the incoming rays of  $\phi_{\text{max}} = 5^\circ$ ,  $ij$  terms such that  $c_{i,j}^{\xi} \phi^i / (2f^j \Delta\xi) > 10^{-3}$  and  $c_{i,j}^{\eta} \phi^i / (2f^j \Delta\eta) > 10^{-3}$ .

As we apply the same conditions to spherical prime-focus design, less terms are present at higher order, i.e. less spherical aberration. To mirror the result for the ideal Davies-Cotton, several non leading terms are added giving a consistent picture for both developments as shown in Table A.1.

*Comparisons.* A comparison between exact (numerically calculated) results and the presented limited Taylor development for both designs is presented in Fig. A.7.

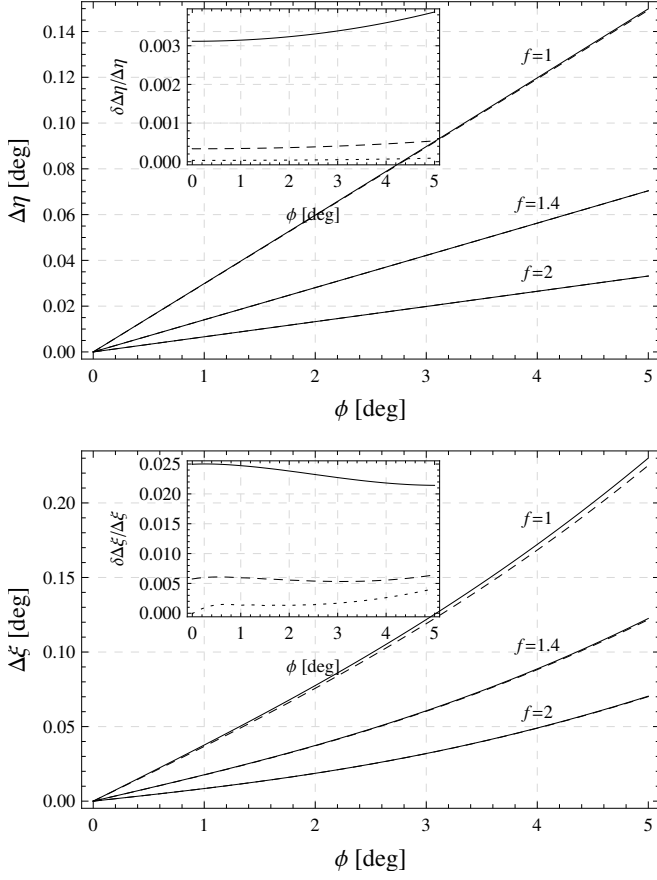


Figure A.7: Comparison between the exact (solid), i.e. numerically calculated, resolution parameters  $\Delta\xi$  and  $\Delta\eta$  and the result of the limited Taylor development (dashed). The inset shows the ratio of both for  $f = \{1.0, 1.4, 2.0\}$  (solid, dashd, dotted).

In [16] and [17], 3<sup>rd</sup> order developments for the Davies-Cotton and spherical mirror, respectively, have been discussed. The obtained coefficients are repeated here for completeness in table A.1. Both solutions show up to 20% fractional error  $\delta\Delta\eta$ , e.g. at  $f = 1$ .

While in [17], terms  $x^i y^j \phi^k$  in the development were kept only to the 3<sup>rd</sup> order, i.e.  $i + j \leq 3$ , here terms were kept up to  $i + j \leq 5$  and  $k \leq 3$ .

At the expense of the introduction of more terms, consequently, the precision of the presented development is about ten times better as illustrated in Fig. A.8.

*Obscuration.* In the above considerations, the shadow of a possible detector in the focal plane has been neglected. By changing the lower bound from  $r = 0$  to  $r = 5^\circ \cdot f$  in expressions A.8, obscuration can easily be quantified. Fig. A.9 shows that obscuration degrades the resolution parameters by about 1.5% at  $f = 1$  up to about 6% at  $f = 2$ ,  $5^\circ$  off-axis.

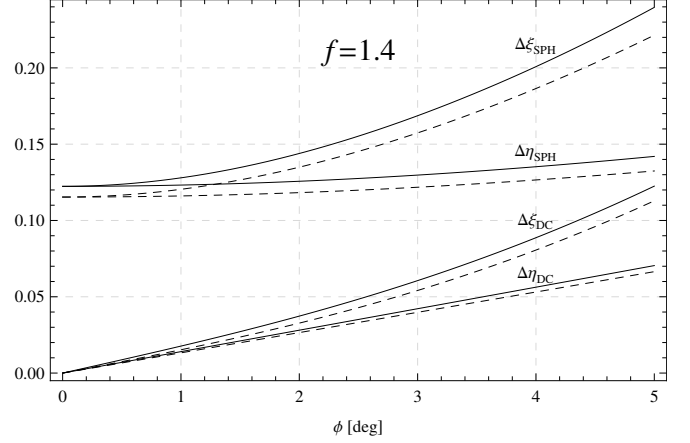


Figure A.8: Comparison between the exact, i.e. numerically calculated, resolution parameters  $\Delta\xi$  and  $\Delta\eta$  and the result of the limited Taylor development from [17] and [16].

### Appendix A.2. Parameterization for a tessellated reflector

A realistic implementation of the non-constructable Davies-Cotton telescope consists in introducing a reflector made of multiple individual spherical mirrors. The tessellation number is defined as the number  $N$  of mirrors in the diagonal. In the limit  $N = \infty$ , it is identical to the ideal Davies-Cotton design. In practice,  $N$  is a number  $\lesssim 30$ .

*Simulation.* The effective parametrization is presented as a correction to the limited Taylor development derived earlier. The correction is implemented through ray-tracing simulation performed with the MARS software (described in [18, 19, 20]), which do fully reproduce the results obtained earlier in the case of a spherical and ideal Davies-Cotton reflectors. Although an ideal Davies-Cotton reflector cannot be build in reality, it can be simulated easily. Simulations enable the use of arbitrary tessellation, since analytical solution being not very well suited for this task.

For the simulation the following properties have been used:

- Individual mirrors are hexagonal. For symmetry reasons each hexagon is rotated by  $15^\circ$  against the  $x/y$ -axis
- The mirrors are fixed on a hexagonal grid in the  $x/y$ -plane with spacing  $d$
- The diameter of the individual mirrors is defined as  $nd^2 = \pi D^2 / \sqrt{3}$ , with  $n$  being the total number of mirrors in the system
- Their center is located on a sphere around the focal point (this corresponds to  $f_{DC}$  for the ideal Davies-Cotton)
- The focal length  $F$  of each mirror is equal to the radius of the sphere, and therefore equal to the focal length of the system
- The overall shape of the reflector is also hexagon like
- The tessellation number  $N$  is the number of mirrors in the diagonal
- Each mirror is oriented to a virtual point in  $2F$  (this corresponds to  $n_{DC}$  for the ideal Davies-Cotton)

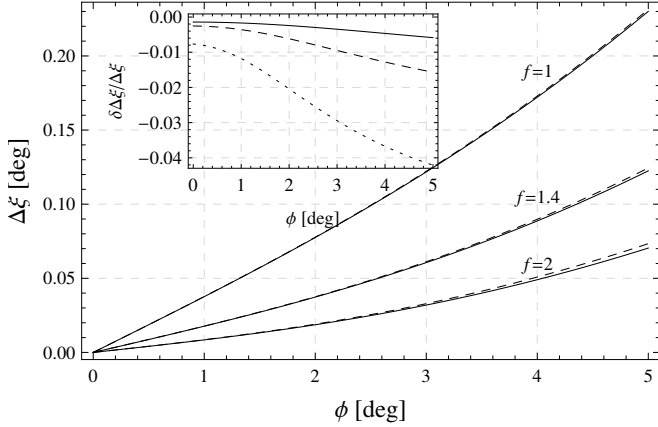
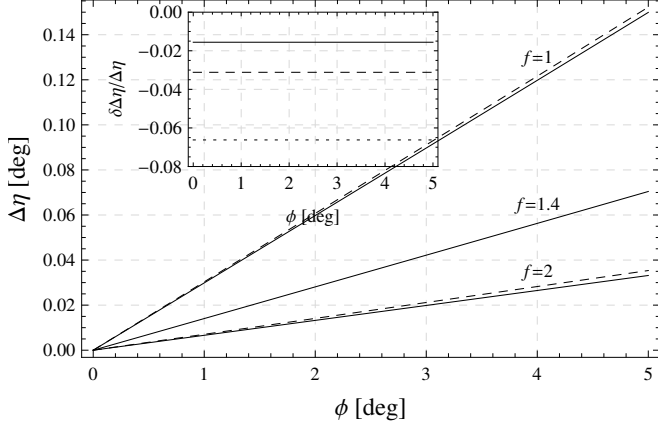


Figure A.9: Resolution parameters  $\Delta\xi$  and  $\Delta\eta$  of the exact results, i.e. numerically calculated, with (dashed) and without (solid) obscuration. Inset shows the ratio of both for  $f = \{1, 1.4, 2\}$  (solid, dashed, dotted).

- The small effect of obscuration by the focal instrumentation is neglected
- The mirror surface is assumed to be ideal

An example for such a reflector is given in Fig. A.10

Simulations have been carried out for  $N$  between 1 and 79 in steps of two, in the range  $1 \leq F/D \leq 2$  in steps of 0.1 and for rays with off-axis angles comprised in  $0^\circ \leq \phi \leq 6.5^\circ$  in steps of  $0.5^\circ$ .

Empirically, it could be found that introducing a dependence on the tessellation number, the formulas given in Appendix A.1 for the spherical mirror and the ideal Davies-Cotton mirror could be unified. For this, a linear dependence at 0<sup>th</sup> order in  $\phi$ , and a quadratically at order  $\phi^i$  for  $i \neq 0$ , has been introduced. Additionally, an effective rescaling  $f_{\text{eff}} = f/w$  is needed to reach an accuracy about 5% in the whole simulated range. The root-mean-square of a tessellated Davies-Cotton can then be written as

$$\begin{aligned} \Delta\xi^2 &= \frac{1}{2^4} \left( \sum_j \frac{s_{0,j}^\xi}{N^2 f_{\text{eff}}^j} + \sum_{i>0,j} \left[ \frac{s_{i,j}^\xi - d_{i,j}^\xi}{N} + d_{i,j}^\xi \right] \frac{\phi^i}{f_{\text{eff}}^j} \right), \\ \Delta\eta^2 &= \frac{1}{2^4} \left( \sum_j \frac{s_{0,j}^\eta}{N^2 f_{\text{eff}}^j} + \sum_{i>0,j} \left[ \frac{s_{i,j}^\eta - d_{i,j}^\eta}{N} + d_{i,j}^\eta \right] \frac{\phi^i}{f_{\text{eff}}^j} \right). \end{aligned} \quad (\text{A.11})$$

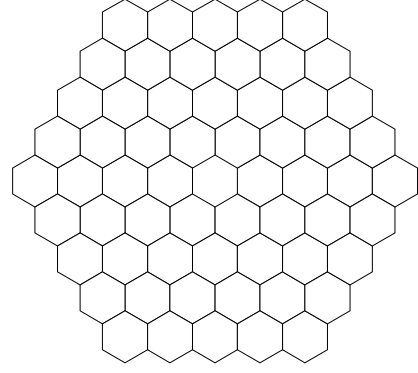


Figure A.10: An example of a reflector layout for  $N=9$  mirrors on the diagonal. This also includes  $N=\{3, 5, 7\}$  removing the rows of outer mirrors consecutively.

The coefficients  $s_{i,j}$  and  $d_{i,j}$  are the ones given in Table A.1 for the spherical and the ideal Davies-Cotton, respectively.

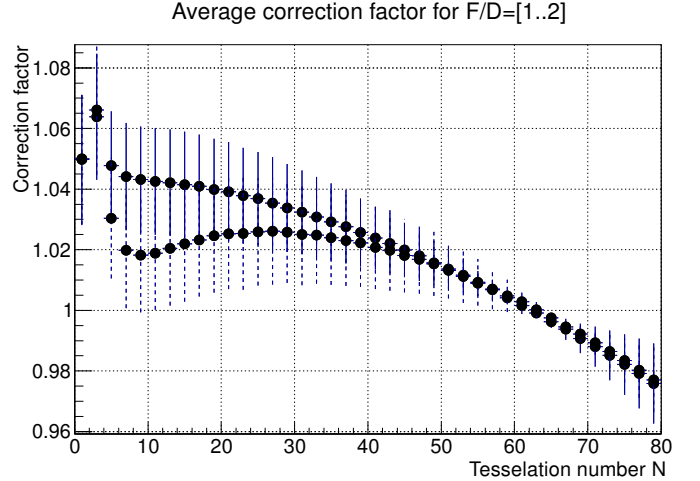


Figure A.11: The scale factor  $w$  as defined by formula A.11 determined from fits to the simulated point-spread function. Each point is the average of all correction factors obtained for the simulated range of  $F/D$ . The error bar denotes the spread. The two curves are the tangential (upper curve, solid) and sagittal (lower curve, dashed), respectively.

The tessellation number  $N$  can here be interpreted as a parameter describing the transition from a single spherical mirror to an ideal Davies-Cotton reflector. The rescaling factor  $w$  can be interpreted as the deviation of the shape from the ideal case. Its value was determined by minimizing the residual, i.e.  $\chi^2$ , between simulated point-spread function and approximated root-mean-square. The differences of the sagittal and tangential residual are minimized independently for each  $N$ . Its value is depicted in Fig. A.11. The introduction of this scale factor effectively reduced the residual from a maximum of 12% to less than 5% for tessellation numbers smaller than 40. Fig. A.12 shows the distribution of the residuals for different tessellation numbers.

Note that for the case  $N = 1$  the simulated single mirror is of hexagonal shape while the analytical approximation de-

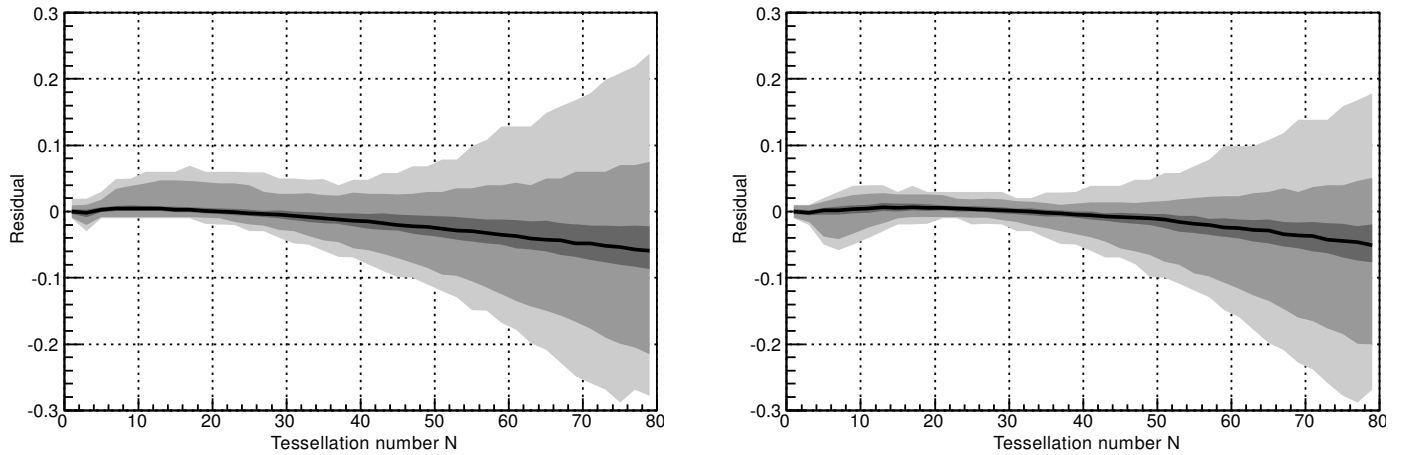


Figure A.12: Relative residual between the result of Eqs. A.11 and the simulated point-spread function after application of the correction factor  $w$  in the range  $F/D=[1,2]$  and  $\alpha=[1,6.5]$ . The black lines corresponds to the median of the distribution. The gray shaded areas to 68%, 95%, and 100% of the distribution. The higher deviations at high tessellation ratios are located around small field-of-views ( $\alpha < 3.5^\circ$ ) and small  $F/D \lesssim 1.3$ . The left and the right plot show the sagittal and the tangential component, respectively.

scribes a disc-like mirror. For cases  $N \gg 1$  the properties of the simulated reflector converge to the ideal Davies-Cotton. While the presented development was calculated for a disc shaped reflector, here, the simulated Davies-Cotton converge to an ideal hexagon. Consequently, in both cases the rescaling factor is expected to be different from unity.

In general, it is not expected to obtain a perfect match between the analytical approximation and the simulation, because simulations will always take into account effect which cannot be easily described analytically, like rays lost between individual mirrors.

From Eqs. A.11 it is evident that for rays with small incident angles the point-spread function is dominated by the 0<sup>th</sup>-order term which decreases fast with high tessellation number. At higher incident angles the point-spread function is dominated by higher order terms which only turn from the spherical to the ideal Davies-Cotton solution for increasing tessellation numbers. In general the dominating term for reasonable incident angles is the 0<sup>th</sup>-order term. Consequently, the point-spread function dramatically improves for  $N > 1$  but for  $N \geq 5$  changes become unimportant. Hence, for practical purposes a single mirror and the case of  $N = 3$  can be excluded while for most practical purposes  $N = 5$  will already be enough.

### Appendix A.3. Summary

It is possible to describe the optical quality of a set of well defined Davies-Cotton reflectors quite well in a single analytical formula. Even the real Davies-Cotton might be slightly different, e.g. different mirror or reflector shapes or obscuration by the focal plane instrumentation, this gives a very good estimate of the optical performance.

### References

- [1] Aharonian, F., Heusler, A., Hofmann, W., *et al.*, 1995, *Journal of Physics G Nuclear Physics*, 21, 985.
- [2] Stamatescu, V., Rowell, G. P., Denman, J., *et al.*, 2011, *Astropart. Phys.*, 34, 886.
- [3] Bernlöhr, K. 2008, *Astropart. Phys.*, 30, 149.
- [4] Schliesser, A., and Mirzoyan, R., 2005, *Astropart. Phys.*, 24, 382.
- [5] Actis, M., Agnetta, G., Aharonian, F., *et al.*, 2011, *Experimental Astronomy*, 32, 193.
- [6] R. Winston, J. C. Minano, P. Benitz, *Nonimaging optics*, 2004, Elsevier Academic Press.
- [7] Braun, I., *et al.*, 2009, In Proc. of the 31<sup>st</sup> International Cosmic Ray Conference.
- [8] Huber, B., Braun, I., *et al.*, 2011, In Proc. of the 32<sup>nd</sup> International Cosmic Ray Conference.
- [9] Anderhub, H., Backes, M., Biland, A., *et al.* 2011, *Nuclear Instruments and Methods in Physics Research A*, 628, 107.
- [10] Aliu, E., Anderhub, H., Antonelli, L. A., *et al.*, 2009, *Astropart. Phys.*, 30, 293.
- [11] Anderhub, H., Backes, M., Biland, A., *et al.*, 2012, Proc. of the 5<sup>th</sup> International Symposium on High-Energy Gamma-Ray Astronomy (*in press*).
- [12] MPPC Multi-Pixel Photon Counters, 2008, HAMAMATSU.
- [13] Chris R. Benn and Sara L. Ellison, *La Palma Night-Sky Brightness*.
- [14] A. K. Konopelko, 1997, *Towards a Major Atmospheric Cerenkov Detector V*, 208.
- [15] Davies, J. M., and Cotton, E. S., 1957, *J. Solar Energy Sci. and Eng.*, 1, 16.
- [16] Vassiliev V., Fegan S., Brousseau P., 2007, *Astropart. Phys.*, 28, 10.
- [17] Schliesser A., Mirzoyan R., 2005, *Astropart. Phys.*, 24, 382.
- [18] Bretz, T. and Wagner, R., 2003, In Proc. of the 28<sup>th</sup> International Cosmic Ray Conference, 5, 2947.
- [19] Bretz, T., 2005, *High Energy Gamma-Ray Astronomy*, 745, 730.
- [20] Bretz, T. and Dorner, D., 2008, *American Institute of Physics Conference Series*, 1085, 664.